Aerosol Measurements in the Troposphere and Stratosphere

L. Elterman

Light scattering measurements from a searchlight beam were carried out in New Mexico to determine the aerosol properties of the atmosphere. Although data were acquired to an altitude of about 70 km, the results show the aerosol attenuation parameters to be significant to about 35 km. The expression for the aerosol attenuation coefficient is derived based on the field geometry in conjunction with Rayleigh and aerosol scattering considerations. The results are categorized into *moderate-structured, medium-structured* and *full-structured* aerosol profiles. Examples of each are discussed and measurements presented which show variation over a 6-h period. A quantitative examination is made of the 20-km aerosol layer. Also, a *medium-structured* profile is selected and treated more extensively to provide preliminary information pertaining to atmospheric scattering and transmission. Ultimately, the data accumulated will provide a substantial number of profiles that will form a basis for various atmospheric studies.

I. Introduction

A knowledge of atmospheric aerosol properties is necessary for the solution of many research and applied problems. Transmission, visibility, astronomical seeing, meteorological tracing, and turbulence are a few important examples. In nearly all of the problems concerned with the interaction of light with the atmosphere, the aerosol attenuation coefficient in the troposphere and stratosphere emerges as an indispensable and little-known parameter. The purpose of the investigation is to determine quantitatively this and related parameters using the searchlight technique. Although measurement capability at 0.55 μ wavelength is about 70 km, the altitudes of interest will be restricted up to 35 km because above this altitude the measurements show that aerosol attenuation can be neglected.

There has been much emphasis on aircraft, balloons, and rockets in the pursuit of this research discipline. However, ground-based remote sensing methods have great merit. First, they have the important capability of performing true *in situ* measurements. Then there is the added advantage of being able to acquire large quantities of data hour after hour and day after day at relatively small cost.

Measurement of twilight intensity as a ground-based technique for aerosol studies was used by Bigg[1], Rozenberg[2], and Volz and Goody.[3] It has, however, some distinct limitations. The method entails long slant paths (about 1000 km), sampling of inordinately large scattering volumes (20 km wide as an example), the use of the angular portion of the phase function which slopes steeply, and generally the need for a multiplicity of assumptions.

Aerosol measurements using the searchlight technique were pioneered by Hulburt[4] who photographed the beam. The results indicated aerosol scattering to an altitude of 11 km. The bibliography of USSR workers in this field is considerable. Prominent is the work of Khvostikov[5] and Rozenberg[6] who used photographic, polarization, and photoelectric methods. The work of the Russian investigators was limited by the omission of beam modulation—one of the important requirements for this type of research. A clear atmosphere and sites at altitudes above ground haze are other necessary factors for reproducibility of the measurements. Detection of aerosol concentrations by using a ruby laser has been reported by Grams and Fiocco[7], by Clemesha *et al.*[8] and by Collis and Ligda.[9]

In this paper, the method for conducting aerosol measurements with searchlight probing is developed. The aerosol attenuation coefficient as a function of altitude is the primary objective. Observations were started in New Mexico in December 1963. The instrumentation, measurement procedures, data processing, and a portion of the results for 0.55 μ are now finalized and will provide the substance for the material to follow.

II. The Energy Transfer Equations

Figure 1 presents the searchlight scene geometry. The projecting mirror is parabolic with a diameter of 91.4 cm; its elevation angle is fixed. The collecting mirror is identical and scans up or down the beam with elevation angle ϕ_d. The beam and field of view are

The author is with CRO, AFCRL, Bedford, Massachusetts 01731.

Received 25 May 1966.

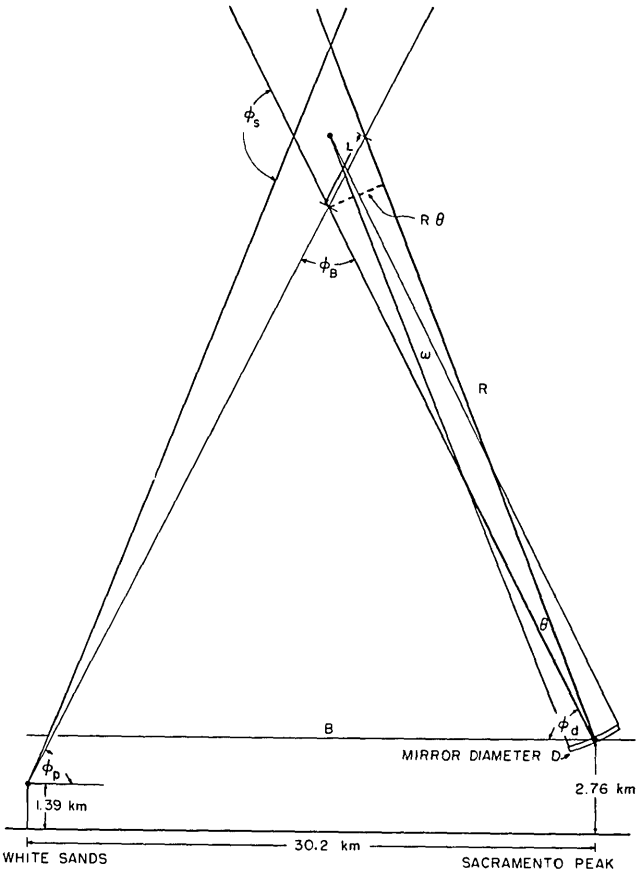

Fig. 1. Searchlight scene geometry in New Mexico. Projector elevation angle $\phi_p = 75°$; beam and collector field divergences are adjusted to 1.7° and 2.0°, respectively. Both divergences are exaggerated in this figure.

aligned in order to be coplanar for all elevation angles. Approximately 30 min is required for a continuous scan of the beam over the altitude range 2.8 km to 35.3 km (0° to 57° elevation). The altitude of the scattering volume is established by the intersection of the optical axis of the beam and the collector field of view. The altitude resolution averages about 1 km. A partial list of the geometrical relationships is shown in Table I.

Since the divergences of the beam and collecting field are small, the opposing extremities of the scattering volume are nearly equal, both angularly and in length. From the scene geometry (Fig. 1), the equations for the energy transfer are as follows:

(a) source to scattering volume

$$F_s \times T_s = EA, \tag{1}$$

where F_s = total energy of source (W), T_s = transmission (molecular + aerosol) source to scatter volume, A = area (normal to beam axis) at scattering volume, receiving incident radiation (cm²), and E = radiance incident on area A (W/cm²);

(b) at the scattering volume

$$J(\phi_s) = EAL\beta(\phi_s), \tag{2}$$

where ϕ_s = scattering angle, $J(\phi_s)$ = intensity of angularly scattered light (W/sr), $\beta(\phi_s)$ = (molecular + aerosol) volume scattering function (cm^{-1}), and L = length of scattering volume (cm);

(c) scattering volume to detector

$$F_d = J(\phi_s)T_d\omega, \tag{3}$$

where F_d = total energy at detector (W), T_d = transmission (molecular + aerosol) scatter volume to detector, and ω = solid angle subtended by collector with apex at element of scattering volume (sr).

Combining Eqs. (1), (2), and (3), the energy at the detector is

$$F_d = F_sT_sT_dL\omega\beta(\phi_s). \tag{4}$$

From Fig. 1 it follows that the product $L\omega$ is constant, i.e.,

$$L = R\theta/\sin\phi_B \tag{5}$$

$$\sin\phi_B = B\sin\phi_p/R \tag{6}$$

$$\omega = (\pi D^2/4R^2). \tag{7}$$

And combining Eqs. (5), (6), and (7),

$$L\omega = (\pi D^2\theta/4B\sin\phi_p) = C_1. \tag{8}$$

Here $\phi_p = 75°$ and C_1 is the constant.

The instrumentation response to the scattered energy is linear, so $E_{rp} = C_2F_d$. Also, measurements show that the variation of source intensity for each scan is small, so F_s can be assigned the constant C_3. If the constants are combined so $C = C_1C_2C_3$, Eq. (4) becomes

$$E_{rp} = CT_sT_d\beta(\phi_s). \tag{9}$$

Rearranging the transmissions and expressing the volume scattering function by its components,

$$T_sT_d = T_rT_p \tag{10}$$

and

$$\beta(\phi_s) = \beta_rP_r(\phi_s) + \beta_pP_p(\phi_s). \tag{11}$$

The definitions are T_s = total transmission source to scatter volume, T_d = total transmission detector to scatter volume, T_r = Rayleigh transmission for both slant paths, T_p = aerosol transmission for both slant paths, β_r = Rayleigh attenuation coefficient (cm^{-1}), β_p = aerosol attenuation coefficient (cm^{-1}), $P_r(\phi_s)$ = normalized Rayleigh phase function (sr^{-1}), and $P_p(\phi_s)$ = normalized aerosol phase function (sr^{-1}). Eq. (9) takes the form

$$E_{rp} = CT_rT_p[\beta_r \times P_r(\phi_s) + \beta_p \times P_p(\phi_s)], \tag{12}$$

where E_{rp} = instrumentation response (V) and C = proportionality constant (V cm sr).

III. The Aerosol Scattering Equation and Its Solution

Equation (12) has the limitation that the constant C is unknown. The procedure for evaluating C is demonstrated by referring to Fig. 2 which represents a set of measurements obtained 8 May 1964 at 03:05.

Table I. Computer Output (Partial Tabulation) Measurement on 13 April 1964 at 00:18

Collector elevation (degrees) ϕ_d	Scatter volume altitude (km)	Scatter angle (degrees) ϕ_s	Detector response (normalized) E_{rp}	Rayleigh coefficient β_r (km^{-1})	Aerosol coefficient β_p (km^{-1})
0	2.76	75	93.95	8.852×10^{-3}	9.50×10^{-3}
1	3.28	76	89.20	8.396	9.72
—	—	—	—	—	—
—	—	—	—	—	—
—	—	—	—	—	—
20	12.65	95	23.49×10^{0}	2.674	5.74×10^{-4}
21	13.14	96	22.03	2.478	5.85
22	13.63	97	20.93	2.291	7.49
23	14.13	98	19.83	2.117	8.79
24	14.63	99	19.26	1.962	1.20×10^{-3}
25	15.12	100	18.53	1.812	1.45
26	15.63	101	17.80	1.675	1.66
27	16.13	102	16.34	1.547	1.44
28	16.64	103	14.87	1.428	1.17
29	17.16	104	13.73	1.319	1.03
30	17.67	105	12.89	1.214	1.04
31	18.20	106	11.95	1.122	9.33×10^{-4}
32	18.73	107	11.17	1.031	9.09
33	19.26	108	10.23	9.491×10^{-4}	7.63
34	19.80	109	95.10×10^{-1}	8.715	7.20
35	20.35	110	88.38	7.940	7.08
36	20.90	111	81.19	7.301	6.06
37	21.46	112	73.07	6.662	4.44
38	22.03	113	66.87	6.114	3.49
39	22.61	114	62.05	5.567	3.46
40	23.20	115	55.91	5.065	2.40
—	—	—	—	—	—
—	—	—	—	—	—
—	—	—	—	—	—
57	35.28	132	10.00×10^{-1}	7.711×10^{-5}	0.00 (neglected)

The ordinate is designated as the relative response since these values are normalized to unity at 35.3 km. Also shown is the calculated Rayleigh response for identical conditions. As in other measurements, the curves nearly converge over the last few kilometers. Accordingly, at about 35 km, aerosol scattering is assumed to be sufficiently small so that it can be neglected. Then Eq. (12) for these conditions becomes

$$E_{rp}(35) = CT_r(35)T_p(35)\beta_r(35)P_r(132°). \quad (13)$$

Here 132° corresponds to the scattering angle for the 35.3-km altitude. Combining Eqs. (12) and (13), the altitude variation of the aerosol attenuation coefficient is expressed by

$$\beta_p(h) = \frac{E_{rp}(h)}{E_{rp}(35)} \frac{T_r(35)}{T_r(h)} \frac{T_p(35)}{T_p(h)} \beta_r(35) \frac{P_r(132°)}{P_p(\phi_s)} - \beta_r(h) \frac{P_r(\phi_s)}{P_p(\phi_s)}. \quad (14)$$

As mentioned, the terms $E_{rp}(h)$ and E_{rp} (35) are obtained from the measurements. All the Rayleigh terms are calculated by using the atmospheric attenuation model tabulations[10,11] for 0.55 μ wavelength. The Rayleigh phase function is $P_r(\phi_s) = 0.75\ (1 + \cos^2\phi_s)$. Assuming for the present that the aerosol phase function is established, then Eq. (14) has one unknown because $T_p(h)$ can be expressed in terms of $\beta_p(h)$:

$$T_p(h) = \exp - \sum_{2.76}^{h} \bar{\beta}_p(h)\Delta h \sec Z(h), \quad (15)$$

where $\bar{\beta}_p$ = mean value of β_p for the atmospheric layer (km^{-1}), Δh = layer thickness (km), and $Z(h)$ = sum of the secants of the zenith angles for the beam and collector field slant paths.

Since β_p exists in the transmission term as an exponential, the solution of Eq. (14) is not analytic. The method used is an iterative-convergent procedure. The iteration is started by using the atmospheric attenuation model[10,11] for 0.55 μ to calculate an initial series of aerosol transmission values $T_p(h)$ applicable to the field geometry. Having done this, the model values of $T_p(h)$ have no further function. The iteration procedes as shown in Fig. 3 until convergence is attained. Eq. (14) then yields a final set of $\beta_p(h)$.

As to the choice of the aerosol phase function $P_p(\phi_s)$, the literature is extensive with both computational and experimental studies. Here must be considered the work of Waldram[12], Reeger and Siedentopf[13], Bullrich

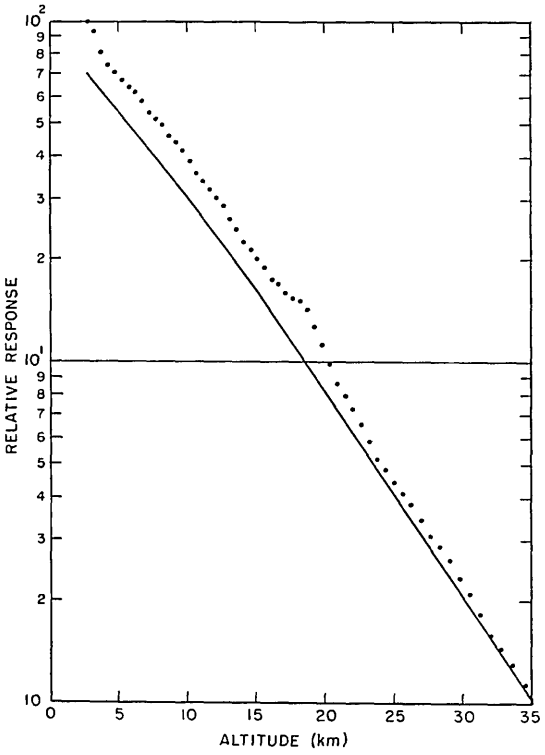

Fig. 2. Instrumentation response of single scan and corresponding Rayleigh values. Wavelength is 0.55 μ. 8 May 1964. 03:05. . . . data points (automatically plotted). —— calculated Rayleigh response.

and Möeller[14,15], Foitzik and Zschaeck[16], Deirmendjian[17], Fraser[18], Barteneva[19] and others who made important contributions to this area of research. The criteria finally considered for the choice of the phase function were (1) that its derivation should be from field measurements with a meteorological range of at least 30 km, and (2) that the phase function should permit Eq. (14) to converge within a reasonable number of iterations. The results of Reeger and Siedentopf (and there are others) readily meet these criteria. The aerosol phase function was derived from their measurements (see Fig. 4).

IV. Instrumentation

The methods follow those used previously[20,21] but with considerable modification. The beam intensity is modulated by a shutter mechanism fronting the searchlight, as shown in Fig. 5. The modulation, 20 c/s, represents a compromise between a desired high modulation frequency and the mechanical spin limitation of the shutters. An auxiliary detector, mounted on the beam modulator, monitors the source intensity and generates a signal which is synchronous with the modulation. The synchronous signal is transmitted to a site 30.2 km distant, where the optical collector, synchronous detector, and amplifier are located. The collector mirror and the photomultiplier assembly comprise the sensing device. The detector-filter response peaks at 0.55 μ and has a wavelength bandwidth at the half-amplitude response approximating 550 Å.

V. Sky Background

The measurements were conducted during moonless nights so the sky background would be minimized. Although modulation of the beam contributes greatly to isolating the desired scattering from the sky background and other spurious sources, it does not completely effect isolation. The sources of the background level are (a) the star field and airglow (direct and scattered), (b) secondary and higher order scattering from the beam, and (c) instrumentation noise.

Probably the major source is direct and scattered light from the star field and the night airglow. Beam modulation with synchronous rectification is effective in suppressing these sources, but not entirely so. The incidence of modulated and unmodulated energy on the photomultiplier results in a shot noise spectrum, part of which is passed by the bandwidth of the amplifier (0.02 c/s). Secondary and higher order scattering from the beam enters the field of the collector mirror for the most part at low altitudes (regions of relatively high atmospheric molecular density), but is considered small due to 30.2-km separation of the sites. Finally, the photomultiplier dark current and other instrumentation noise contribute to the signal background. The signal-to-noise ratio at 35 km exceeds twenty and increases rapidly at lower altitudes.

VI. Observations and Results

The data obtained is in the form of a continuous trace on the chart recorder. The elevation angle ϕ_d is recorded automatically on the chart along with the response to the scattered light. Subsequently, the response is digitized at 1° intervals as in Table I. The results based on sampling of a year's measurements show that it is convenient to categorize the aerosol distributions derived from the data, into *moderate-structured*, *medium-structured* and *full-structured* profiles.

Following through on the measurements discussed in Fig. 2, the response values were used in Eq. (14) and the resulting aerosol attenuation coefficients were plotted automatically from the punch card computer output, as shown in Fig. 6. The Rayleigh coefficients and the extinction coefficients (Rayleigh + aerosol) are included. The character of the aerosol curve places it in the category of a *medium-structured* profile. Since the aerosol coefficients primarily are proportional

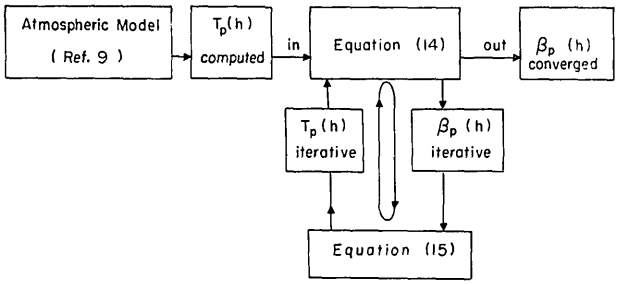

Fig. 3. Iteration procedure. T_p is aerosol transmission. β_p is aerosol attenuation coefficient.

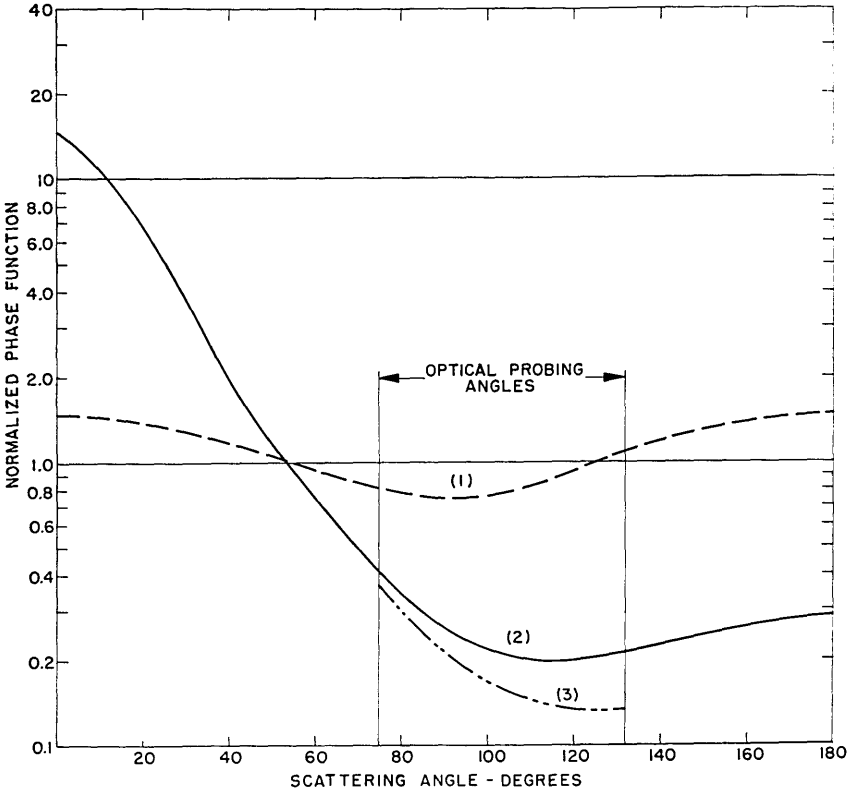

Fig. 4. Phase functions. (1) — — Rayleigh. (2) ——Reeger and Seidentopf met. range = 30 km. (3) — - - — aerosol, derived from (2).

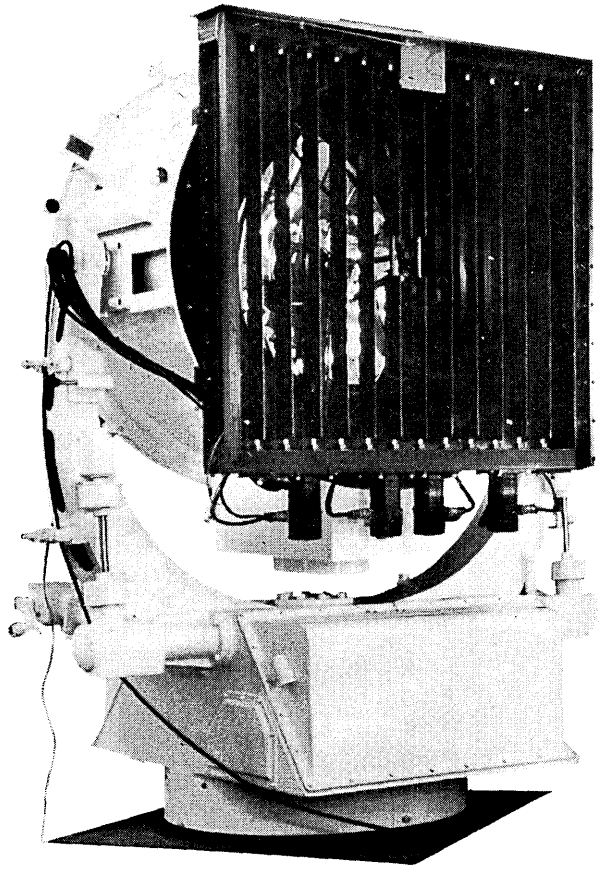

Fig. 5. Modulating shutters with drive motors below. Detector assembly for synchronous rectification mounted near the top.

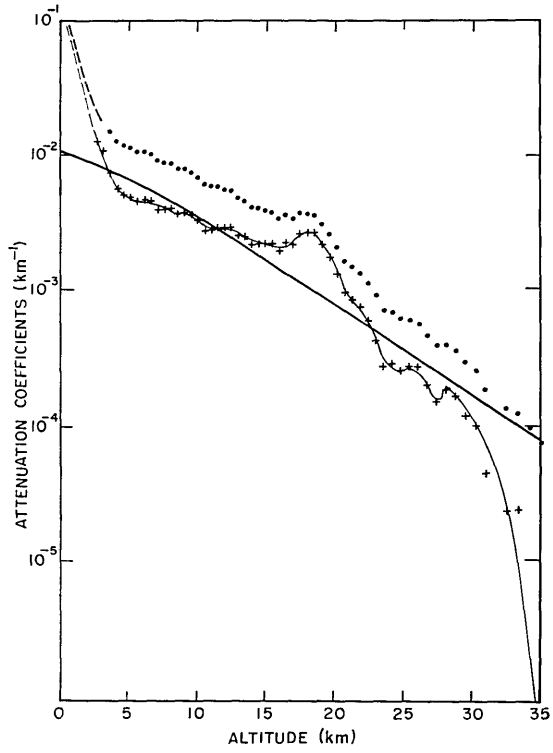

Fig. 6. Aerosol and related parameters. The aerosol profile represents the *medium-structured* category. 8 May 1964. 03:05. —— Rayleigh (computed). +++ aerosol (from measurements with smoothing). ··· extinction (Rayleigh and aerosol). - - - extrapolated (in accordance with Ref. 9).

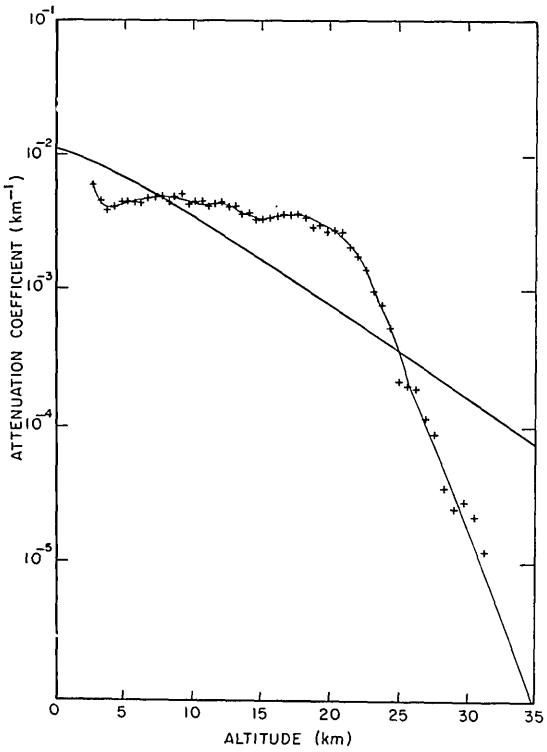

Fig. 7. Aerosol profile representing the *moderate-structured* category. 17 December 1963. 02:00. —— Rayleigh (computed). +++ aerosol (from measurements with smoothing).

to the aerosol number density, the profiles are discussed accordingly. The aerosol density drop over the lowest few kilometers is usual. The diminution then is relatively smooth to 16 km and is followed by a region of aerosol concentration with a maximum at 18 km. For the region 2.8 km down to sea level, extrapolation was carried out to conform with the 0.55 μ tabulations of the atmospheric attenuation model.[9]

The profile in Fig. 7 is an example from the *moderate-structured* category. Here the aerosol number densities between 4 km and 15 km show relatively little change. The identity of the 20-km layer is poorly defined.

The staggered scale presentation in Fig. 8 shows a series of profiles taken over a 6-h period. These profiles are categorized as *full-structured*. This body of data was obtained consecutively except for periods of interim activity pertaining to operational requirements. The low altitude concentration shows a maximum at 5 km in profiles A, B, and C. During the night, the maximum becomes less defined and in profile E acquires a simple logarithmic distribution (2.8–6.5 km). Next, a tropopause concentration with a maximum at about 9 km is evident, but this region increasingly loses its identity in profiles D and E. There follows a region of aerosol concentration above the tropopause (12–23 km) which persists through the night. It may well be identified with the 20-km aerosol layer determined by the direct measurements of Junge *et al.* [22] Finally, a 26-km maximum shows surprising temporal integrity. Above 28 km, the decreasing values indicate a quasi-Rayleigh atmosphere.

The usefulness of the $\beta_p(h)$ profile for obtaining quantitative information can be readily demonstrated. In Fig. 8, profile C, the aerosol concentration usually designated as the 20-km layer, can be examined with considerable detail. It is well-defined, asymmetrical, and extends in altitude from 12.7 km to 23.2 km (Table I). The median of the layer occurs at 18.2 km where $\beta_p = 9.33 \times 10^{-4}$ km^{-1} and the turbidity factor, $\beta_p/\beta_r = 0.83$. The maximum aerosol density, however, occurs at 15.6 km where $\beta_p = 1.66 \times 10^{-3}$ km^{-1} and the turbidity factor is 0.99. The aerosol optical thickness of the layer is determined by

$$\tau_p = \sum_{12.7}^{23.2} \bar{\beta}_p(h)\Delta h, \qquad (16)$$

where $\bar{\beta}_p(h)$ is the mean aerosol attenuation coefficient (km^{-1}) for each altitude increment, and Δh is the altitude increment (km) as designated in Table I. This leads to the value $\tau_p = 0.01$ which is modest but important in applications requiring large zenith angles. The slant path transmissions through the layer due to Rayleigh and aerosol attenuation were obtained with Eq. (15) and are shown in Fig. 9.

VII. Error Considerations

Here, it will be convenient to designate a set of measured values $E_{rp}(h)$ as the input profile and the computed aerosol attenuation coefficients $\beta_p(h)$ as the output profile.

Examination of Eq. (14) shows that the term E_{rp} (35) can bear significantly on the accuracy of the results. It is necessary, therefore, to consider the effect of noise and background on this term. If the background level causes E_{rp} (35) to increase, some negative values in the output profile may result. This is because the measured and Rayleigh curves (as shown in Fig. 2) are nearly converged between 30 km and 35

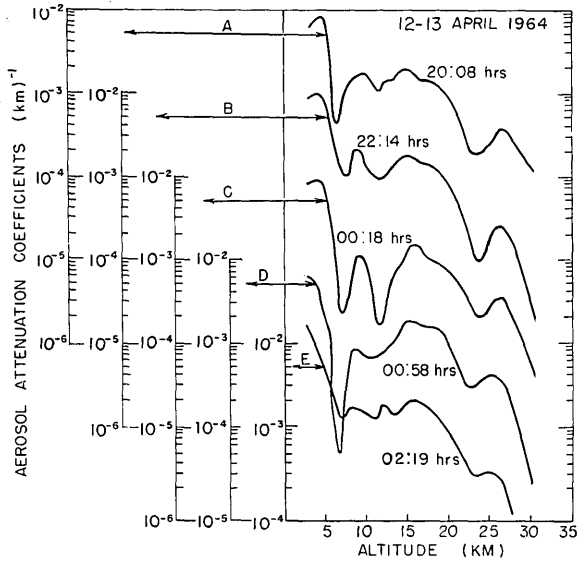

Fig. 8. Aerosol profiles representing the *full-structured* category showing variations over a period of about 6 h.

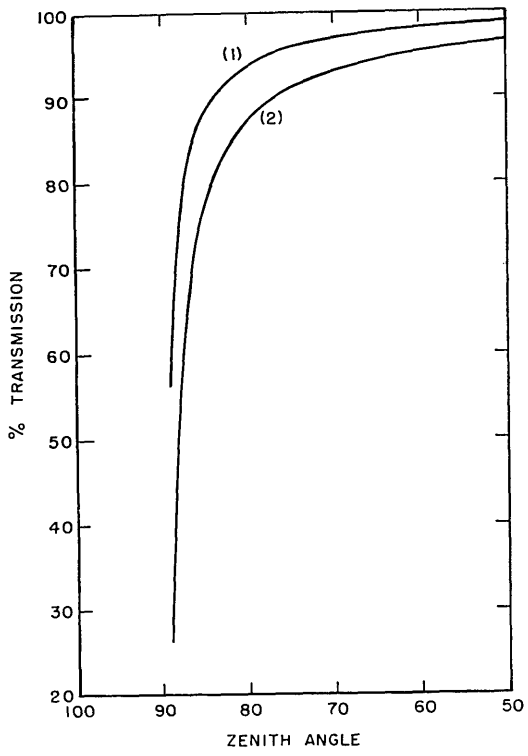

Fig. 9. Slant path transmission (0.55 μ) through 20-km aerosol layer. 13 April 1964 at 00:18. (1) Aerosol. (2) Rayleigh + aerosol.

km. Then the presence of noise may cause the measured value to be less than the corresponding Rayleigh value which is an unacceptable condition. Accordingly, the procedure was adopted where the input profile is smoothed for the last few kilometers. The computer then examines the derived $\beta_p(h)$ values after the first iteration for the presence of negative values. Routinely, the instrumentation is set so the measured value of E_{rp} (35) is near unity. If any negative values are present, E_{rp} (35) is reduced repeatedly by 0.001 until only positive values of $\beta_p(h)$ exist. The iteration then continues with no further adjustments until convergence is obtained. This procedure effectively corrects E_{rp} (35) for noise and background.

The angular pointing error when scanning the beam upward or downward approximates $\pm 0.1°$. This is equivalent to an error of 0.05 km to 0.09 km, depending on the altitudes of measurement.

It is reasonable to estimate that the other functional aspects of the measurements can result in about 5% or 6% error in the $E_{rp}(h)$ values. If systematic (always negative or positive), this percentage applies to the entire input profile, and the resulting output profile will be unaffected because we are dealing with ratios, $E_{rp}(h)/E_{rp}$ (35). However, a part of the input profile subjected to a 5% change results in considerable error due to the summation procedure, Eq. (15). This is demonstrated by choosing a severe example of error simulation, i.e., increasing the $E_{rp}(h)$ values over a substantial portion of the input profile (approximately 27 km) of Table I. If these are increased by 5%, the output profile values change 28% at 2.76 km and 40% at 29.7 km. A corresponding 6% increase results in changes from 33% to 48%.

In instances where convergence cannot be attained, the data is abandoned. Usually, failure to converge is attributed to high values of $E_{rp}(h)$ for altitudes under 5 km, caused by heavy dust or thin clouds.

VIII. Concluding Remarks

The results discussed may be considered representative, but there are some reservations. This is because they were selected rather than based on averages. A substantial number of measurements now comprise a data bank that will be used for atmospheric transmission studies. The material also has good potential for other investigations such as nocturnal and seasonal trends of aerosol concentrations, effects of volcanic action, correlation studies with radiosonde and ozonesonde measurements.

An understanding of the atmospheric processes involved is best obtained with a sampling as large as possible. Results and interpretation based on data in quantity will be the subject of a future paper.

The author would like to acknowledge the fine assistance with instrumentation afforded by A. B. Campbell and J. R. Yoder, the helpful review provided by R. Penndorf, R. W. Fenn and R. G. Walker, the able assistance by M. Jones with field activities; also, his appreciation to J. V. Dave for contributing a long afternoon of discussion during our 1964 visit to Leningrad, to C. Atwood and others who assisted with data reduction, to M. G. Hurwitz, R. Hoffman and J. Fusco for their participation with computer programming, and to W. Daunt, J. Lee, H. Bass, and M. M. Kielman who were dedicated to acquiring every minute of useful data.

References

1. E. K. Bigg, Tellus **16,** 2 (1964).
2. G. V. Rozenberg, *Twilight* (Plenum Press, Inc., New York, 1966).
3. F. E. Volz and R. M. Goody, J. Atmospheric Sci. **19,** 385 (1962).
4. E. O. Hulburt, J. Opt. Soc. Am. **27,** 377 (1946).
5. I. A. Khvostikov, Bull. Acad. Sci. USSR Phys. Ser. **10,** 4 (1946).
6. G. V. Rozenberg, "Searchlight Beam in the Atmosphere," (Izd.-VO, Akad. Nauk, SSSR, Moscow, 1960).
7. G. Fiocco and G. Grams, J. Atmospheric Sci. **21,** 3 (1964).
8. B. R. Clemesha, G. S. Kent, and R. W. H. Wright, Nature **209,** 184 (1966).
9. R. T. H. Collis and M. G. H. Ligda, J. Atmospheric Sci. **23,** 255 (1966).
10. L. Elterman, Appl. Opt. **3,** 1139 (1964).
11. L. Elterman, "Atmospheric Attentuation Model, 1964, in the Ultraviolet, Visible and Infrared Regions for Altitudes to 50 km," Rept. AFCRL-64-740, Air Force Cambridge Research Laboratories, Bedford, Mass. (1964).
12. J. M. Waldram, Quart. J. Roy. Meteorol. Soc. **71,** 319 (1945).
13. E. Reeger and H. Siedentopf, Optik **1,** 15 (1946).
14. K. Bullrich and F. Möeller, Optik **2,** 301 (1947).
15. K. Bullrich, Advan. Geophys. **10,** 99 (1964).
16. L. Foitzik and H. Zschaeck, Zeit. Meteorol., **7,** 1 (1952).
17. D. Deirmendjian, Appl. Opt. **3,** 157 (1964).

18. R. S. Fraser, "Scattering Properties of Atmospheric Aerosols", Rept. AFCRC-TN-60-256, Air Force Cambridge Research Laboratories, Bedford, Mass. (1960).
19. O. D. Barteneva, Bull. Acad. Sci. USSR, Geophys. Ser. **1**, 1852 (1960).
20. L. Elterman, "Searchlight Probing Technique for Upper Atmosphere Measurements", in *Encyclopaedic Dictionary of Physics*, J. Thewlis, Ed. (Pergamon Press, Inc., New York, 1962).
21. L. Elterman and A. B. Campbell, J. Atmospheric Sci. **21**, 457 (1964).
22. C. E. Junge, C. W. Chagnon, and J. E. Manson, J. Meteorol. **18**, 81 (1961).